



Chinese Pharmaceutical Association
Institute of Materia Medica, Chinese Academy of Medical Sciences

Acta Pharmaceutica Sinica B

www.elsevier.com/locate/apsb
www.sciencedirect.com



ORIGINAL ARTICLE

Aureane-type sesquiterpene tetraketides as a novel class of immunomodulators with interleukin-17A inhibitory activity

Xin Tang^{a,d,†}, Chuanxi Wang^{b,†}, Lei Wang^{c,f,†}, Feifei Ren^d,
Runqiao Kuang^b, Zhenhua Li^{a,d}, Xue Han^b, Yiming Chen^d,
Guodong Chen^b, Xiuqing Wu^d, Jie Liu^c, Hengwen Yang^d,
Xingzhong Liu^e, Chen Wang^{c,*}, Hao Gao^{b,*}, Zhinan Yin^{a,d,*}

^aGuangdong Provincial Key Laboratory of Tumor Interventional Diagnosis and Treatment, Zhuhai Institute of Translational Medicine, Zhuhai People's Hospital Affiliated with Jinan University, Jinan University, Zhuhai 519000, China

^bInstitute of Traditional Chinese Medicine and Natural Products, College of Pharmacy/Guangdong Province Key Laboratory of Pharmacodynamic Constituents of TCM and New Drugs Research/International Cooperative Laboratory of Traditional Chinese Medicine Modernization and Innovative Drug Development of Ministry of Education (MOE) of China, Jinan University, Guangzhou 510632, China

^cDepartment of Respiratory, Capital Medical University, Beijing 100069, China

^dBiomedical Translational Research Institute, Health Science Center (School of Medicine), Jinan University, Guangzhou 510632, China

^eState Key Laboratory of Mycology, Institute of Microbiology, Chinese Academy of Sciences, Beijing 100190, China

^fDepartment of Respiratory and Critical Care Medicine, the Second Affiliated Hospital of Xi'an Jiaotong University (Xibei Hospital), Xi'an 710004, China

Received 1 December 2022; received in revised form 19 February 2023; accepted 13 March 2023

KEY WORDS

Aureane-type
sesquiterpene
tetraketides;
IL-17A;

Abstract Interleukin (IL)-17A, a pro-inflammatory cytokine, is a fundamental function in the onset and advancement of multiple immune diseases. To uncover the primary compounds with IL-17A inhibitory activity, a large-scale screening of the library of traditional Chinese medicine constituents and microbial secondary metabolites was conducted using splenic cells from IL-17A-GFP reporter mice cultured under Th17-priming conditions. Our results indicated that some aureane-type sesquiterpene tetraketides isolated

*Corresponding authors.

E-mail addresses: cyh-birm@263.net (Chen Wang), tghao@jnu.edu.cn (Hao Gao), tzhinan@jnu.edu.cn (Zhinan Yin).

†These authors made equal contributions to this work.

Peer review under the responsibility of Chinese Pharmaceutical Association and Institute of Materia Medica, Chinese Academy of Medical Sciences.

<https://doi.org/10.1016/j.apsb.2023.03.017>

2211-3835 © 2023 Chinese Pharmaceutical Association and Institute of Materia Medica, Chinese Academy of Medical Sciences. Production and hosting by Elsevier B.V. This is an open access article under the CC BY-NC-ND license (<http://creativecommons.org/licenses/by-nc-nd/4.0/>).



Experimental autoimmune encephalomyelitis;
Pulmonary hypertension

from a wetland mud-derived fungus, *Myrothecium gramineum*, showed remarkable IL-17A inhibitory activity. Nine new aureane-type sesquiterpene tetraketides, myrogramins A–I (**1**, **4**–**11**), and two known ones (**2** and **3**) were isolated and identified from the strain. Compounds **1**, **3**, **4**, **10**, and **11** exhibited significant IL-17A inhibitory activity. Among them, compound **3**, with a high fermentation yield dose-dependently inhibited the generation of IL-17A and suppressed glycolysis in splenic cells under Th17-priming conditions. Strikingly, compound **3** suppressed immunopathology in both IL-17A-mediated animal models of experimental autoimmune encephalomyelitis and pulmonary hypertension. Our results revealed that aureane-type sesquiterpene tetraketides are a novel class of immunomodulators with IL-17A inhibitory activity, and hold great promise applications in treating IL-17A-mediated immune diseases.

© 2023 Chinese Pharmaceutical Association and Institute of Materia Medica, Chinese Academy of Medical Sciences. Production and hosting by Elsevier B.V. This is an open access article under the CC BY-NC-ND license (<http://creativecommons.org/licenses/by-nc-nd/4.0/>).

1. Introduction

The interleukin (IL)-17 family of cytokines comprises IL-17A to IL-17 F, and the former is the founding member of this family¹. IL-17A is typically produced under inflammatory conditions by T helper 17 (Th17) cells, a critical subclass of CD4⁺ T cells first identified in 2005^{2,3}. Retinoid-related orphan nuclear receptor γ (ROR γ t) is a major transcriptional factor regulating the transcription of *Il17a*, in turn triggering Th17 cell differentiation^{3,4}.

IL-17A, a pro-inflammatory cytokine, has been widely investigated for its involvement in multiple inflammatory and autoimmune disorders such as psoriasis, axial spondylitis, multiple sclerosis (MS), rheumatoid arthritis, systemic lupus erythematosus, and pulmonary hypertension (PH), lacking effective intervention in therapies^{5–8}. MS is an autoimmune disease of the central nervous system (CNS) and it is hallmarked by the loss of myelin sheath and neuronal degeneration. It results in multiple clinical manifestations and comorbidities, including unilateral optic neuritis, sensory disturbances, and depression⁹. The experimental autoimmune encephalomyelitis (EAE) animal model can mimic human MS and serves as a classical disease model to study the pathogenicity of IL-17A and Th17^{10,11}. PH is a set of disorders with a hallmark of elevated blood pressure in the pulmonary arteries¹². Accumulating evidences suggest a significant correlation between IL-17A level and PH development^{8,13,14}. Our previous study showed that a neutralizing antibody against IL-17A and IL-17A knockout mice could reduce hypoxia-induced PH index, while exogenous recombinant mouse (rm) IL-17A can further aggravated the disease¹⁵.

Given the pathogenicity of IL-17A in inflammatory and autoimmune disorders, multiple studies have attempted to target IL-17A for treating immune-related diseases. Ixekizumab and secukinumab, neutralizing antibodies against IL-17A, have been approved for treating psoriasis, axial spondylitis, and psoriatic arthritis^{16,17}. However, the application of these antibodies is limited due to their multiple shortcomings, including compromised tissue penetration, low persistence, undesired administration routes, typically long half-life, and high cost. For such reasons, small molecule drugs with distinct advantages, are proposed to be superior to antibodies¹⁸. Therefore, the development of small molecule immunomodulators targeting IL-17A is

necessitated as they may hold the potential to improve the clinical treatment of IL-17A-based immunotherapies along with expanding more clinical indications.

Currently, no small molecule modulators targeting IL-17A have been approved. Small molecule inhibitors with skeletal diversity and direct binding to ROR γ t that initiates *Il17a* transcription, have been developed, and clinical trials for treating inflammatory disorders are underway¹⁹. Nonetheless, due to the limited effectiveness of topical administration and safety concerns associated with the oral administration of these drugs, there is a high attrition rate in clinical trials²⁰. Over the last decade, small molecule inhibitors with similar scaffolds targeting the IL-17A/IL-17 RA protein-protein interaction have been developed. For instance, LEO 153339, LY3509754, and DC-806 are representative compounds in phase I clinical trials¹⁸. Among them, LY3509754 has been discontinued due to the apparent hepatotoxicity induction. Notably, phase II clinical trial for MYMD-1, a small molecule modulator indirectly inhibiting IL-17A, is still underway²¹. Hence, small molecule screening of novel modulators with IL-17A inhibitory activity is a promising area of direction.

Our group constructed a library of traditional Chinese medicine constituents and microbial metabolites comprising nearly 300 natural products. To identify small molecules that regulate immune activity by inhibiting IL-17A expression, the compounds from this library were screened using an *ex vivo* screening platform based on IL-17A-green fluorescent protein (GFP) reporter mice. Of all the small molecules showing IL-17A inhibitory activity, a class of aureane-type sesquiterpene tetraketides derived from a wetland mud-derived fungus, *Myrothecium gramineum* (ZLW0801-19), captured our attention. A total of nine new aureane-type sesquiterpene tetraketides, myrogramins A–I (**1**, **4**–**11**), and two known ones (**2** and **3**) were isolated from this fungal strain. Compounds **1**, **3**, **4**, **10**, and **11** showed significant IL-17A inhibitory activity, which could be a novel class of immunomodulators.

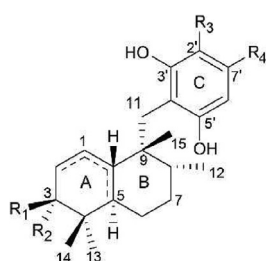
Herein, we demonstrated the separation and structural elucidation of these aureane-type sesquiterpene tetraketides, along with their ability to suppress IL-17A activity. Furthermore, we conducted a preliminary *in vitro* mechanism of the representative aureane-type sesquiterpene tetraketides **3** and its efficacy evaluation of the EAE and PH animal models.

2. Results

2.1. Isolation and structural elucidation of aureane-type sesquiterpene tetraketides from *Myrothecium gramineum*

The strain ZLW0801-19 was isolated from the mud and obtained from Zhalong Wetland, Heilongjiang Province, China. Premised on its morphological traits as well as its ribosomal internal transcribed spacer, the strain was determined to be *M. gramineum* (GenBank accession JX077058.1). The fungus was cultured on a rice solid medium. Following the completion of the fermentation process, the culture was extracted thrice with EtOAc. An unpurified extract was obtained after evaporating the organic solvent under decreased pressure, which was exposed to silica-gel, octadecylsilane (ODS), and preparative/semi-preparative high-performance liquid chromatography (HPLC) to produce 11 aureane-type sesquiterpene tetraketides (**1–11**). The structures of these compounds (Fig. 1) were elucidated by using single-crystal X-ray diffraction, electronic circular dichroism (ECD) spectra, 1D/2D nuclear magnetic resonance (NMR), and high-resolution electrospray ionization mass spectrometry (HR-ESI-MS).

Compound **1** was obtained as a colorless crystal plate. The chemical formula of compound **1** was identified as C₂₃H₃₂O₄ (8 degrees of unsaturation) based on the quasi-molecular ion detected at *m/z* 373.2379 [M + H]⁺ by HR-ESI-MS. The ¹³C NMR spectrum exhibited 23 carbon signals conforming to the chemical formula of the compound. In conjunction with the Distortionless Enhancement by Polarization Transfer 135 (DEPT 135) experiment, these carbons were classified as one carbonyl (δ_C 193.5), eight olefinic or aromatic carbons [comprising two *sp*² methine carbons (δ_C 116.3 and 109.8)], two *sp*³ quaternary carbons (δ_C 43.7 and 36.9), three *sp*³ methine carbons [including one oxygenated *sp*³ methine carbon (δ_C 71.5)], four *sp*³ methylene carbons (δ_C 31.6, 30.3, 26.6, and 23.2), and five methyl carbons (δ_C 25.2, 22.9, 17.7, 17.2, and 14.8). The ¹H NMR spectrum demonstrated the existence of one aldehyde hydrogen [δ_H 9.94



1	R ₁ = OH	R ₂ = H	R ₃ = CHO	R ₄ = CH ₃	$\Delta^{1(10)}$
2	R ₁ = OAc	R ₂ = H	R ₃ = CHO	R ₄ = CH ₂ OH	$\Delta^{1(10)}$
3	R ₁ = OH	R ₂ = H	R ₃ = CHO	R ₄ = CH ₂ OH	$\Delta^{1(10)}$
4	R ₁ = OH	R ₂ = H	R ₃ = CHO	R ₄ = CH ₂ OAc	$\Delta^{1(10)}$
5	R ₁ = OAc	R ₂ = H	R ₃ = CHO	R ₄ = CH ₂ OAc	$\Delta^{1(10)}$
6	R ₁ = OH	R ₂ = H	R ₃ = CHO	R ₄ = CHO	$\Delta^{1(10)}$
7	R ₁ = OH	R ₂ = H	R ₃ = CHO	R ₄ = CH(OCH ₃) ₂	$\Delta^{1(10)}$
8	R ₁ = OH	R ₂ = H	R ₃ , R ₄ = 2'-CH ₂ NHCO-7'		$\Delta^{1(10)}$
9	R ₁ , R ₂ = O		R ₃ = CHO	R ₄ = CH ₂ OH	$\Delta^{1(2)}$
10	R ₁ = OH	R ₂ = H	R ₃ = CHO	R ₄ = CH ₂ OH	$\Delta^{5(10)}$
11	R ₁ = OAc	R ₂ = H	R ₃ = CHO	R ₄ = CH ₂ OH	$\Delta^{5(10)}$

Figure 1 Chemical structures of aureane-type sesquiterpene tetraketides (**1–11**).

(1H, s)], two aromatic or olefinic protons [δ_H 6.23 (1H, s) and 4.89 (1H)], and five groups of methyl protons [δ_H 2.42 (3H, s), 1.03 (3H, d, *J* = 6.6 Hz), 0.95 (3H, s), 0.91 (3H, s), and 0.59 (3H, s)]. During the experiment based on heteronuclear single quantum coherence (HSQC), all non-exchangeable proton resonance frequencies were observed to be connected with the directly bonded carbon atoms. The ¹H–¹H COSY experiment revealed the existence of two isolated spin systems (C-1–C-2–C-3–OH-3 and C-5–C-6–C-7–C-8–C-12), as depicted in Fig. 2A. The planar structure of compound **1** was revealed when the critical heteronuclear multiple bond correlation (HMBC) correlations were combined with the two deduced spin systems, degrees of unsaturation, as well as chemical shifts (Fig. 2A). Supporting Information Table S1 depicts the assignments for all of the resonances of protons and carbons. The rotating frame Overhauser effect spectroscopy (ROESY) experiment was used to determine the relative configuration of compound **1** (Fig. 2B). Premised on the ROESY correlations between H-5 and Hb-7/Ha-11, it was determined that H-5/Hb-7/H₂-11 were all distributed within the same side of ring B and adopted an axial orientation. The correlations observed by ROESY between Hb-6 and H-8 imply that Hb-6/H-8 were distributed within the same side of ring B and had an axial orientation of ring B. Based on the correlations found by ROESY between H-5 and H-3, it was determined that H-5/H-3 were distributed on a similar side of ring A. As the connections found by ROESY between Ha-2 and H₃-14, it was determined that both Ha-2 and H-14 were distributed within the same side of ring A. Consequently, the relative configuration of compound **1** was designated as 3*S*^{*}, 5*R*^{*}, 8*R*^{*}, and 9*R*^{*}. The single-crystal X-ray crystallographic analysis of compound **1** (Fig. 2C) was verified the above inference. Moreover, the value of the flack parameter 0.12 (16) made it possible to designate the absolute configuration of compound **1** as 3*S*, 5*R*, 8*R*, and 9*R*. Hence, it was determined that compound **1** had the structure of 2,4-dihydroxy-3-(((1*R*,2*R*,4*aR*,6*S*)-6-hydroxy-1,2,5,5-tetramethyl-1,2,3,4,4*a*,5,6,7-octahydronaphthalen-1-yl)methyl)-6-methylbenzaldehyde and was named myrogramin A.

Compounds **2** and **3**, which has been previously identified²², were determined to be myrothecisins C and D, respectively, based on spectroscopic analysis and comparing their reported spectroscopic data. Additionally, further confirmation of the structure of compound **2** was achieved by examining the X-ray crystallographic data obtained from a single crystal (Fig. 2C).

Compounds **4** and **5** were obtained as solid yellow substances. The fact that compound **4** had a molecular weight that was 42 atomic mass units (C₂H₂O) higher than **3** was suggestive of the possibility that **4** was an acetylated derivative of **3**. The primary HMBC associations from H₂-8'/H₃-10' to C-9' demonstrated that acetylation occurred at the C-8' in **4**. The molecular weight of compound **5** was 42 atomic mass unit (C₂H₂O) higher than that of compound **4**, and the ¹H and ¹³C NMR results were comparable to those of compound **4**, except for the existence of an extra acetyl group [δ_C 169.8/ δ_C 21.0; δ_H 1.98 (3H, s)]. This indicates that **5** was the acetylated derivative of **4**. The primary HMBC correlations from H-3/H₃-17 to C-16, in conjunction with the notable downfield shift of C-3 (from δ_C 71.5 to δ_C 75.5), suggested that **5** was the 3-acetylated derivative of **4**. The examination of the data obtained from 2D NMR (HSQC, ¹H–¹H COSY, HMBC, and ROESY) (Supporting Information Tables S4 and S5) confirmed the deduced structures of **4** and **5**. The assignments for all of the resonances of protons and carbons is mentioned in Tables S4 and S5. Furthermore, compounds **4** and **5** were transformed into **3** after

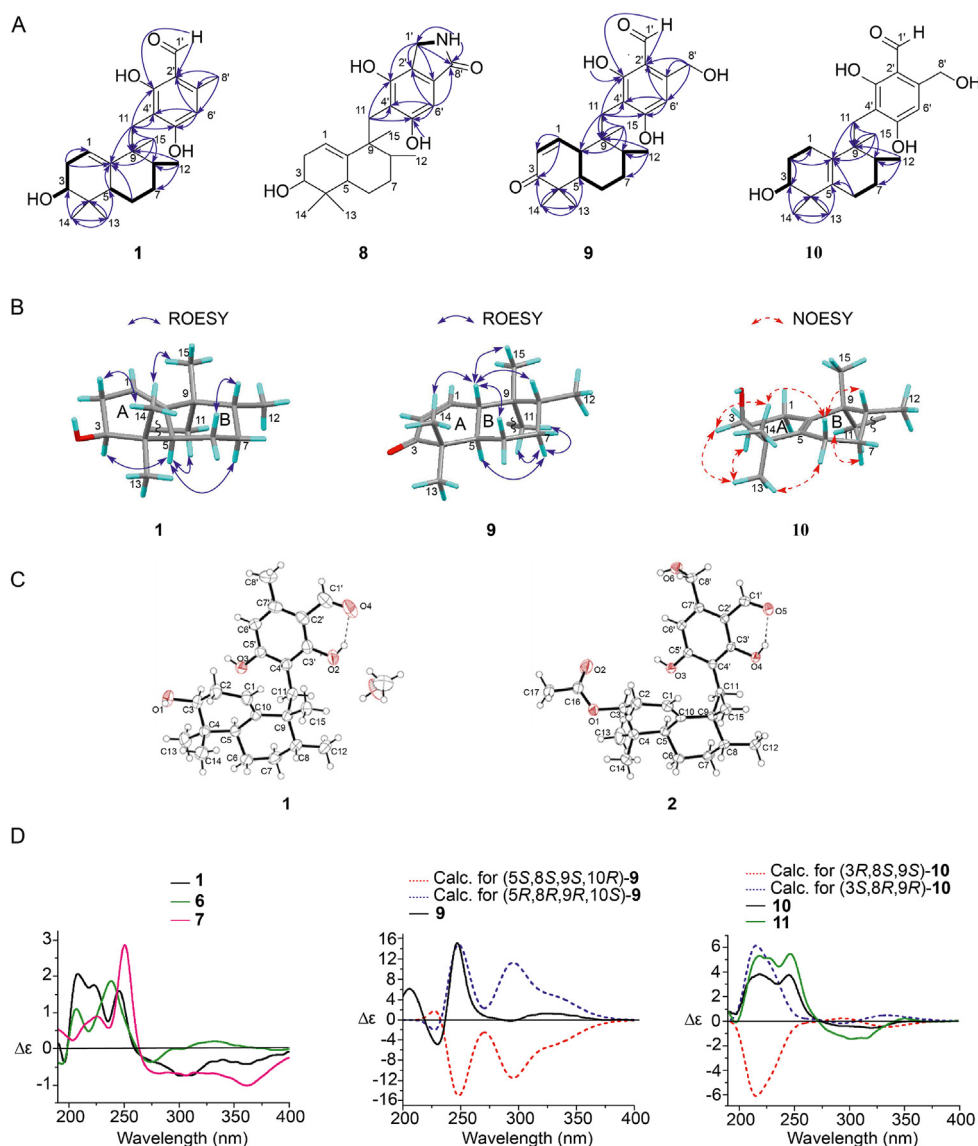


Figure 2 Key images for the structural elucidation of **1**, **2**, and **6–11**. (A) Key ^1H - ^1H COSY (bold in black), HMBC correlations (arrow in blue), and planar structures of compounds **1** and **8–10**. (B) Primary ROESY correlations of compounds **1** and **9**, and primary NOESY correlations of compound **10**. (C) X-Ray structures of compounds **1** and **2**. (D) Experimental ECD spectra of compounds **1**, **6**, **7**, and **9–11** (CH₃OH), and calculated ECD spectra of compounds **9** and **10** (CH₃OH).

hydrolysis using a 2% CH₃ONa/CH₃OH solution, which collaborated with the aforementioned findings. Therefore, the structure of **4** was determined to be 2-formyl-3,5-dihydroxy-4-(((1*R*,2*R*,4*aR*,6*S*)-6-hydroxy-1,2,5,5-tetramethyl-1,2,3,4,4*a*,5,6,7-octahydronaphthalen-1-yl)methyl)benzyl acetate and named as myrogramin B. The structure of **5** was highlighted as 4-(((1*R*,2*R*,4*aR*,6*S*)-6-acetoxy-1,2,5,5-tetramethyl-1,2,3,4,4*a*,5,6,7-octahydronaphthalen-1-yl)methyl)-2-formyl-3,5-dihydroxybenzyl acetate and named as myrogramin C.

Compounds **6** and **7** were obtained as yellow solids. The molecular formulas of these compounds were identified as C₂₃H₃₀O₅ (9 degrees of unsaturation) and C₂₅H₃₆O₆ (8 degrees of unsaturation), respectively, as demonstrated by the quasi-molecular ion at m/z 409.2009 [M + Na]⁺ and 455.2415 [M + Na]⁺ in HR-ESI-MS. The data of ^1H and ^{13}C NMR of **6** were comparable to **1**, except for the methyl at δ_{C} 17.7 (C-8') in compound **1** which was

substituted by an aldehyde group at δ_{C} 192.9 (C-8') in **6**. The structure of **6** was constructed premised on the main HMBC correlations from H-8' to C-2'/C-6'/C-7'. As per the data of the ^1H and ^{13}C NMR spectrometers, compound **7** seemed to be a dimethyl acetal derivative of compound **6**. The primary HMBC correlations from H₃-9'/H₃-10' to C-8', as well as from H-8' to C-2'/C-6'/C-7', suggested that the dimethyl acetal group was located at C-8'. The examination of the data obtained from 2D NMR (HSQC, ^1H - ^1H COSY, and HMBC, Supporting Information Tables S6 and S7) and the chemical formula validated the planar structure of compounds **6** and **7**. Tables S6 and S7 present the complete assignments for all of the proton and carbon resonances. Depending on the ROESY correlations, compounds **6** and **7** were assigned the relative configurations of 3*S**, 5*R**, 8*R**, and 9*R**, which were identical to compound **1**. The ECD experiment showed that the curves of compounds **6** and **7** were similar to

those of compound **1** (Fig. 2D). Considering the coexistence of compounds **6**, **7**, and **1**, it was determined that the absolute configurations of **6** and **7** should be 3*S*, 5*R*, 8*R*, and 9*R*. Therefore, the structure of **6** has been deciphered as follows: 3,5-dihydroxy-4-(((1*R*,2*R*,4*aR*,6*S*)-6-hydroxy-1,2,5,5-tetramethyl-1,2,3,4,4*a*,5,6,7-octahydronaphthalen-1-yl)methyl)phthalaldehyde and was named myrogramin D. Elucidation of the structure of **7** was accomplished as 6-(dimethoxymethyl)-2,4-dihydroxy-3-(((1*R*,2*R*,4*aR*,6*S*)-6-hydroxy-1,2,5,5-tetramethyl-1,2,3,4,4*a*,5,6,7-octahydronaphthalen-1-yl)methyl)benzaldehyde and was named myrogramin E.

Compound **8** was obtained as a green solid. Compound **8**'s molecular formula was deduced to be C₂₃H₃₁NO₄ (9 degrees of unsaturation) premised on the HR-ESI-MS peak located at *m/z* 386.2340 [M + H]⁺. The data obtained from ¹H and ¹³C NMR illustrated that compound **8** had identical sesquiterpene units (from C-1 to C-15) with **1**. Fig. 2A depicted that the ¹H–¹H COSY analysis illustrated the existence of a spin system (H₂-1'–NH). The tetraketide moiety (from C-1' to C-8') was established after considering the HMBC correlations from Ha-11/Hb-11 to C-3'/C-4'/C-5', from H-6' to C-2'/C-4'/C-5'/C-8', from Ha-1'/Hb-1' to C-2'/C-3'/C-7'/C-8', from NH to C-1'/C-8', and from OH-5' to C-5' (Fig. 2A). Evaluation of the 2D NMR data (HSQC, ¹H–¹H COSY, and HMBC) provided additional confirmation of the planar structure of compound **8** (Supporting Information Table S8). It was demonstrated by the ROESY correlations (Table S8) that the relative configuration of compound **8** was comparable to that of **1**. Based on the coexistence of compounds **8** and **1**, the absolute configuration of **8** was designated as 3*S*, 5*R*, 8*R*, and 9*R*. Therefore, the structure of **8** was designated as 4,6-dihydroxy-5-(((1*R*,2*R*,4*aR*,6*S*)-6-hydroxy-1,2,5,5-tetramethyl-1,2,3,4,4*a*,5,6,7-octahydronaphthalen-1-yl)methyl)isoindolin-1-one and was named myrogramin F.

Compound **9** was obtained as a green solid. The quasi-molecular ion detected by HR-ESI-MS at the *m/z* 387.2176 [M + H]⁺ demonstrated that the chemical formula of **9** was C₂₃H₃₀O₅ (9 degrees of unsaturation). As per the ¹³C NMR spectrum of **9**, 23 carbon signals related to the chemical formula of the compound. After the DEPT 135 spectrum was taken into consideration, these carbons were classified as two carbonyls (δ_C 204.1 and 193.8), eight olefinic or aromatic carbons [comprising three *sp*² methine carbons (δ_C 148.9, 127.8, and 107.6)], two *sp*³ quaternary carbons (δ_C 45.2 and 40.6), three *sp*³ methine carbons, four *sp*³ methylene carbons [comprising one oxygenated *sp*³ methylene carbon (δ_C 59.8)], and four methyl carbons (δ_C 24.3, 23.1, 22.1, and 15.8). The data from the ¹H NMR spectrum illustrated the existence of one aldehyde hydrogen [δ_H 9.99 (1H, s)], three aromatic or olefinic protons [δ_H 6.79 (1H, br. d, *J* = 10.5 Hz), 6.59 (1H, s), and 5.78 (1H, dd, *J* = 10.5, 3.2 Hz)], four groups of methyl protons [δ_H 1.08 (3H, s), 0.99 (3H, s), 0.97 (3H, s), and 0.93 (3H, d, *J* = 6.3 Hz)]. In HSQC, all of the non-exchangeable proton resonances were connected to the directly attached carbon atoms. The key ¹H–¹H COSY correlations illustrated the existence of one isolated spin system (C-2–C-1–C-10–C-5–C-6–C-7–C-8–C-12). The HMBC correlations from H-1 to C-2/C-3, from H₃-14 to C-3/C-4/C-13, from H₃-13 to C-4/C-5/C-14, from H₃-12 to C-7/C-8/C-9, from H₃-15 to C-8/C-9/C-10/C-11, from Ha-11/Hb-11 to C-9/C-10/C-3'/C-4'/C-5', from H₂-8' to C-2'/C-6'/C-7', from H-6' to C-2'/C-4'/C-5', from H-1' to C-2'/C-3', and from OH-3' to C-3' illustrated the partial structure of compound **9**. Compound **9**'s planar structure was deduced from its chemical formula and the results of its chemical shift (Fig. 2A). Supporting Information Table S9 displays the assignments for each proton resonance as

well as each carbon resonance. The ROESY correlations between H-10 and H₃-14/Ha-6/H-8 demonstrated that rings A and B were *trans*-fused, suggesting that they were on the same face of the bicyclic system, and H-10/Ha-6/H-8 occupied axial bonds of ring B. The ROESY correlations between Hb-7 and H-5/Ha-11/Hb-11 indicated that Hb-7/H-5 and C-11 were situated within the same face of ring B and on the axial orientation of ring B. As a consequence, it was determined that the relative configuration of **9** should be 5*R**, 8*R**, 9*R**, and 10*S** (Fig. 2B). The predicted ECD curve of (5*R*,8*R*,9*R*,10*S*)-**9** and (5*S*,8*S*,9*S*,10*R*)-**9** were estimated utilizing a quantum chemical approach at the level of [APFD/6-311++G (2 d,p)]. The experimental ECD curve depicted in Fig. 2D was comparable to the projected ECD curve for (5*R*,8*R*,9*R*,10*S*)-**9**. As a result, it was determined that the absolute configuration of **9** was 5*R*, 8*R*, 9*R*, and 10*S*. Hence, the structure of **9** was established as 2,4-dihydroxy-6-(hydroxymethyl)-3-(((1*R*,2*R*,4*aR*,8*aS*)-1,2,5,5-tetramethyl-6-oxo-1,2,3,4,4*a*,5,6,8*a*-octahydronaphthalen-1-yl)methyl)benzaldehyde and was named myrogramin G.

Compound **10** was obtained as a white solid. As evidenced by the quasi-molecular ion detected by HR-ESI-MS with the *m/z* 389.2329 [M + H]⁺, the chemical formula of **10** was established as C₂₃H₃₂O₅ (8 degrees of unsaturation). The data from ¹H and ¹³C NMR revealed that compound **10** had the same tetraketide moiety (from C-1' to C-8') as compound **2**. The analyses of the ¹H–¹H COSY experiment illustrated the existence of two isolated spin systems (C-1–C-2–C-3–OH-3 and C-6–C-7–C-8–C-12). The HMBC correlations from Ha-2/Hb-2 to C-1/C-3/C-10, from H₃-14 to C-3/C-4/C-13, from H₃-13 to C-4/C-5/C-14, from Ha-6/Hb-6 to C-5/C-10, from H₃-12 to C-7/C-8/C-9, from H₃-15 to C-8/C-9/C-10/C-11, and from Ha-11/Hb-11 to C-9/C-10 revealed the sesquiterpene moiety (from C-1 to C-15) of compound **10** (Fig. 2A). The molecular formula, chemical shifts, and 2D NMR data analysis verified the planar structure of compound **10** (Supporting Information Table S10). The nuclear Overhauser effect spectroscopy (NOESY) correlations between Hb-11 and Ha-7 illustrated that they were situated on a similar side of ring B. The NOESY correlations between Ha-6 and H-8 demonstrated that they were situated on a similar side of ring B. The NOESY correlations between H-3 and H₃-14/H₃-13 illustrated that H-3 adopted the equatorial orientation of ring A. Considering the NOESY correlations between Ha-6 and H₃-14, between Hb-6 and H₃-13, and between Ha-2 and H₃-13, the relative configuration of **10** was designated as 3*S**, 8*R**, and 9*R** (Fig. 2B). We utilized a quantum chemical technique at the level of [APFD/6-311++G (2 d,p)] to compute the predicted ECD curve of (3*S*,8*R*,9*R*)-**10** and (3*R*,8*S*,9*S*)-**10**. As illustrated in Fig. 2D, the experimental curve and the predicted ECD curve of (3*S*,8*R*,9*R*)-**10** were quite comparable to one another. Combined with the coexistence of compounds **10** and **2**, the absolute configuration of compound **10** was designated as 3*S*, 8*R*, and 9*R*. Hence, the structure of **10** was deciphered as 2,4-dihydroxy-3-(((1*R*,2*R*,6*S*)-6-hydroxy-1,2,5,5-tetramethyl-1,2,3,4,5,6,7,8-octahydronaphthalen-1-yl)methyl)-6-(hydroxymethyl)benzaldehyde and was named myrogramin H.

Compound **11** was obtained as a white solid. The molecular formula of compound **11** was identified to be C₂₅H₃₄O₆ (9 degrees of unsaturation), as shown by the quasi-molecular ion with *m/z* 453.2246 [M + Na]⁺ in HR-ESI-MS analysis. The fact that compound **11** had a molecular weight that was 42 atomic mass unit (C₂H₂O) higher than **10** suggested that **11** was perhaps an acetylated derivative of **10**. The data from ¹H and ¹³C NMR of **11** were comparable to **10**, except for the additional acetyl group [δ_C

170.1/ δ_C 21.0; δ_H 1.93 (3H, s)]. The primary HMBC correlations from H-3/H₃-17 to C-16 and the significant downfield shift of C-3 (from δ_C 73.0 to δ_C 76.4) indicated acetylation occurred at the OH-3 position in compound **11**. Premised on the comprehensive assessment of 2D NMR data (Supporting Information Table S11), the planar structure of compound **11** was ascertained. The NOESY correlations indicated that the relative configuration of **11** was comparable to compound **10**. Combined with the similar ECD curves of **11** and **10** (Fig. 2D) and the co-existence of **11** and **10**, the absolute configuration of **11** was designated as 3*S*, 8*R*, and 9*R*. Hence, the structure of **11** was determined to be as (2*S*,5*R*,6*R*)-5-(3-formyl-2,6-dihydroxy-4-(hydroxymethyl)benzyl)-1,1,5,6-tetramethyl-1,2,3,4,5,6,7,8-octahydronaphthalen-2-yl acetate and was named myrogramin I.

2.2. Ex vivo screening of aureane-type sesquiterpene tetraketides with IL-17A inhibitory activity

Natural products are an important source of small molecule immunomodulators²³. Ex vivo screening platform based on IL-17A-GFP reporter mice was used to determine the regulatory action of aureane-type sesquiterpene tetraketides from *M. gramineum* on inhibiting the activity of IL-17A. Briefly, splenic cells isolated from IL-17A-GFP reporter mice were cultured in medium supplemented with Th17 cell-associated differentiation factors to make cells conducive to Th17-priming. Cells were exposed to 0.01% DMSO (vehicle control), 10 μ mol/L aureane-type sesquiterpene tetraketides or 1 μ mol/L SR2211 (a ROR γ t inhibitor as positive control compound) at the beginning of the culture. After three days, the proportion of IL-17A-GFP in CD4⁺ T cells was estimated utilizing flow cytometry analysis (Fig. 3A). The screening results revealed that aureane-type sesquiterpene tetraketides **1**, **3**, **4**, **10**, and **11** substantially attenuated IL-17A production in CD4⁺ T cells (Fig. 3B and C). Notably, compounds **3** and **11** showed a better IL-17A inhibitory activity compared to other compounds.

2.3. Assessment of IL-17A inhibitory activity of compound **3** in T cells under Th17-priming conditions

Compounds **3** and **11** displayed IL-17A inhibitory activity in a dosage-dependent way with IC₅₀ values of 3.168 and 3.135 μ mol/L, respectively (Fig. 4A and B). Compound **3** had the highest fermentation productivity and significant IL-17A inhibitory activity among all the compounds **1**–**11**. Hence, compound **3** was selected as a candidate compound to investigate the efficacy and the underlying mechanism. A significant reduction in the IL-17A generation of CD4⁺ T and CD8⁺ T cells was observed in a dosage-dependent manner following three days of treatment with compound **3** (Fig. 4C–F). This indicates that compound **3** could broadly inhibit IL-17A expression in diverse cellular processes. Similarly, the absolute number of CD4⁺IL-17A-GFP⁺ and CD8⁺IL-17A-GFP⁺ T cells decreased considerably when treated with various doses of compound **3** (Fig. 4G and H). Flow cytometry analysis of the ratio of 7-aminoactinomycin D (7-AAD⁺), annexin V⁺, and 7-AAD⁺annexin V⁺ revealed that equal doses of compound **3** did not affect the apoptosis of splenic cells (Fig. 4I–L). Consistently, a decrease in the protein levels of IL-17A was detected by enzyme-linked immunosorbent assay (ELISA) (Fig. 4M) and Western blotting (Fig. 4N) after three days of treatment of compound **3**. To additionally evaluate the transcriptional regulation of IL-17A activity, the expression of ROR γ t,

a major transcriptional factor of *Il17a*, was determined using Western blotting. As expected, compound **3** dose-dependently decreased the expression of transcription factor ROR γ t (Fig. 4N). These results indicate that the inhibitory activity of IL-17A of compound **3** may be attributed to the decreased level of ROR γ t, the core transcription factor of *Il17a*.

2.4. Compound **3** attenuates the bioenergetic signature of glycolysis

To further identify the gene expression signature and signaling pathways involved in inhibiting IL-17A activity by compound **3**, bulk RNA-seq and bioinformatic analysis were conducted. The gene expression signatures of splenic cells under Th17-priming conditions in the presence and in the absence of compound **3** (5 μ mol/L) were compared using bulk RNA-seq analysis. The analysis of differentially expressed genes (DEGs) revealed a substantial reduction in the expression of many Th17-related genes in cells treated with compound **3** (Fig. 5A), which is in line with the data presented beforehand (Figs. 3 and 4). Meanwhile, quantitative real-time polymerase chain reaction (qRT-PCR) verified the downregulation of these Th17-associated genes, including *Il17a*, *Il17f*, *Rorc*, *Rora*, *Irf4*, and *Batf* (Fig. 5B). Furthermore, an analysis of the pathways with significantly enriched DEGs was undertaken using the Kyoto Encyclopedia of Genes and Genomes (KEGG) pathway enrichment technique. Glycolysis/gluconeogenesis had the highest *P*-adj among all the pathways enriched by compound **3** (Fig. 5C). Therefore, we hypothesized that compound **3** treatment may result in an abnormal bioenergetic signature of the glycolysis/gluconeogenesis pathway. To address this, the extracellular acidification rate (ECAR) was measured to evaluate the impact of compound **3** on glycolysis. Indeed, compound **3** had a dose-dependent effect that considerably suppressed glycolysis as well as glycolytic capacity (Fig. 5D–F).

2.5. Compound **3** suppresses immunopathology of EAE

The EAE animal model mimics human MS and is a classic animal model for investigating the pathogenicity of IL-17A^{10,11}. To assess the functional relevance of IL-17A inhibitory activity of compound **3**, the induction of the EAE model was done utilizing myelin oligodendrocyte glycoprotein peptide 35-55 (MOG35-55) peptide and pertussis toxin (PTX) and treated with compound **3** or vehicle twice daily (Fig. 6A). Clinical scores were recorded daily. Mice treated with MOG35-55 and PTX displayed a robust disease course. The clinical scores showed that pathogenesis was significantly alleviated by the treatment with compound **3** (Fig. 6B). Consistent with this, histopathological examination of spinal cord sections after EAE modeling uncovered that inflammatory cell infiltration (Fig. 6C and E), demyelination (Fig. 6D and F), CD4⁺ T cells (Supporting Information Fig. S1A and C), and IL-17A⁺ cells (Fig. S1B and D) were significantly increased. However, these immune pathological damages were improved almost to normal levels after the administration of compound **3**. Infiltration of pro-inflammatory cells in the CNS is an important feature of EAE or MS, especially myelin-specific CD4⁺ T cells generating GM-CSF, IFN- γ , and IL-17A which perform a vital function in inflammation and demyelination²⁴. Consistent with the improvement in EAE phenotype, we also discovered that compound **3** considerably decreased the percentage of IL-17A- and GM-CSF-generating CD4⁺ T cells in the CNS of EAE (Fig. S1E and F). In addition, the

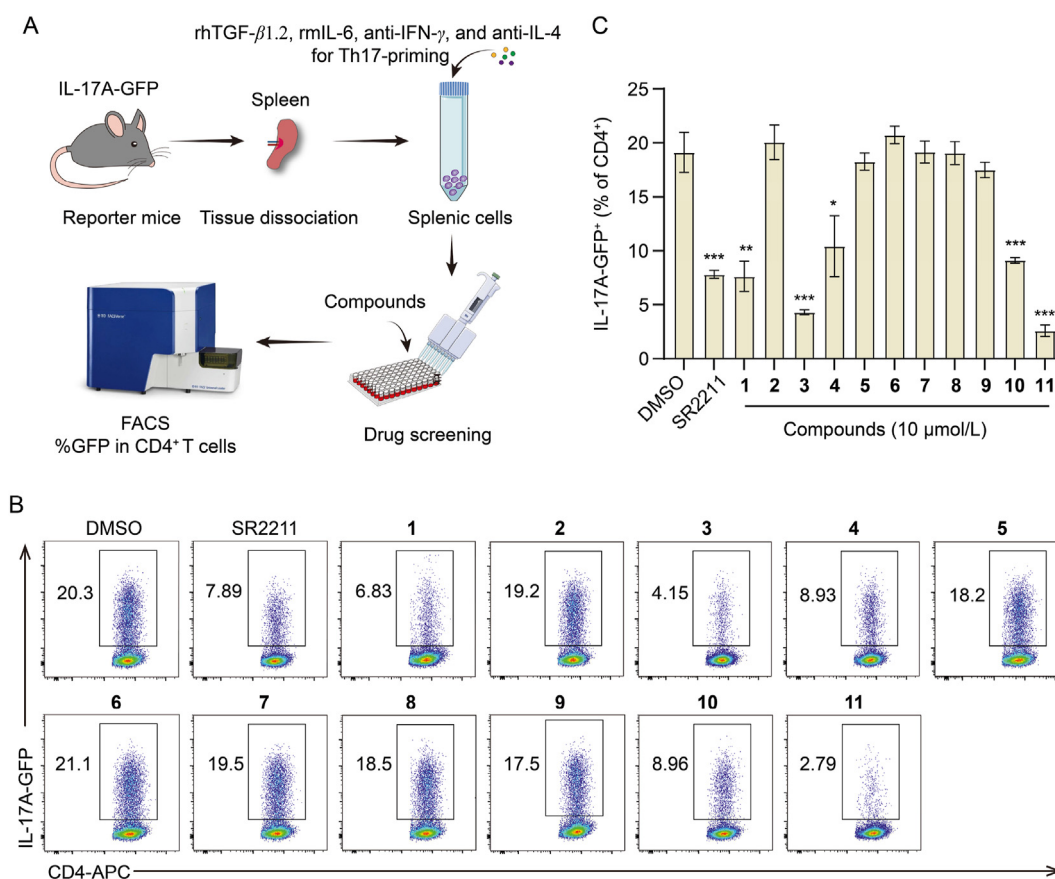


Figure 3 The screening of natural products based on their inhibitory activity of IL-17A. (A) The experimental design of an *ex vivo* screening based on IL-17A-GFP reporter mice. (B) Illustrative flow cytometry plots of IL-17A-GFP gated on CD4⁺ T cells under Th17-priming conditions using splenic cells cultured for three days with 0.01% DMSO, 10 μ mol/L aureane-type sesquiterpene tetraketides, or 1 μ mol/L SR2211. SR2211 is set as a positive control. (C) Statistical histograms of IL-17A-GFP expression in CD4⁺ T cells. Data were reported as mean \pm SD for $n = 3$. * $P < 0.05$, ** $P < 0.01$, *** $P < 0.001$ vs. DMSO group.

treatment of compound **3** contributed to a visual decrease in the absolute number of CD4⁺ IFN- γ ⁺, CD4⁺ GM-CSF⁺, CD4⁺ IL-17A⁺, and CD4⁺ T cells (Fig. S1G).

To further confirm the therapeutic effect of compound **3** on EAE, either compound **3** at a dosage of 40 mg/kg or the vehicle was injected intraperitoneally (ip) twice daily after the clinical score reached 0.5–1 (Fig. 6G). Compound **3** had a restorative effect on the EAE disease model as indicated by the clinical scores (Fig. 6H), histological examination of spinal cord sections (Fig. 6I–L), and infiltration levels of pro-inflammatory immune cells into the CNS (Supporting Information Fig. S2). These results suggest that compound **3** treatment significantly reduces the severity of EAE disease in the initiation and development stages.

2.6. Compound **3** attenuates PH in animal models

Hypoxia-induced PH model is a classical model for studying PH and is hallmarked by elevated pulmonary artery pressure and pulmonary vascular remodeling. The right ventricular systolic pressure (RVSP) was employed to quantify pulmonary artery pressure. When estimating pulmonary arteriolar remodeling, the percentage media thickness (% MT) was calculated. To investigate the efficacy of compound **3** on PH, we established a hypoxia-induced PH model and treated mice with compound **3** at a dosage of 20 mg/kg, twice a week for four weeks. The

experimental schematic is illustrated in Fig. 7A. The data suggested that compound **3** alleviated hypoxia-mediated increase of RVSP (Fig. 7B) and induced intra-pulmonary arteriole (diameters <100 μ m) remodeling (Fig. 7C and D). Similar phenomenon was observed in the monocrotaline (MCT)-induced PH rat model, another classical PH model (Supporting Information Fig. S3). Interestingly, we found that hypoxia-exposed mice treated with compound **3** had a better appetite and gained visible weight compared to untreated hypoxia-exposed mice (Fig. 7E). Further immunohistochemical (IHC) analysis illustrated that the hypoxia-mediated enhancement of IL-17A expression in lung tissues was reversed significantly after treatment with compound **3** (Fig. 7F and G).

3. Discussion

Sesquiterpene polyketides (SPs) are a prominent class of meroterpenoids comprising a sesquiterpene unit and a polyketide-derived moiety^{25,26}. The general sesquiterpene unit contains drimane-type, avarane-type, or aureane-type skeleton²⁶. Based on the number of carbons introduced to the precursor molecule, the polyketide-derived moiety can be divided into triketides, tetraketides, etc.²⁷. SPs show various biological activities, including antioxidant, cytotoxic, antibacterial antiviral, antihyperlipidemic, protein kinase inhibition, and α -glucosidase inhibition^{22,28–33}.

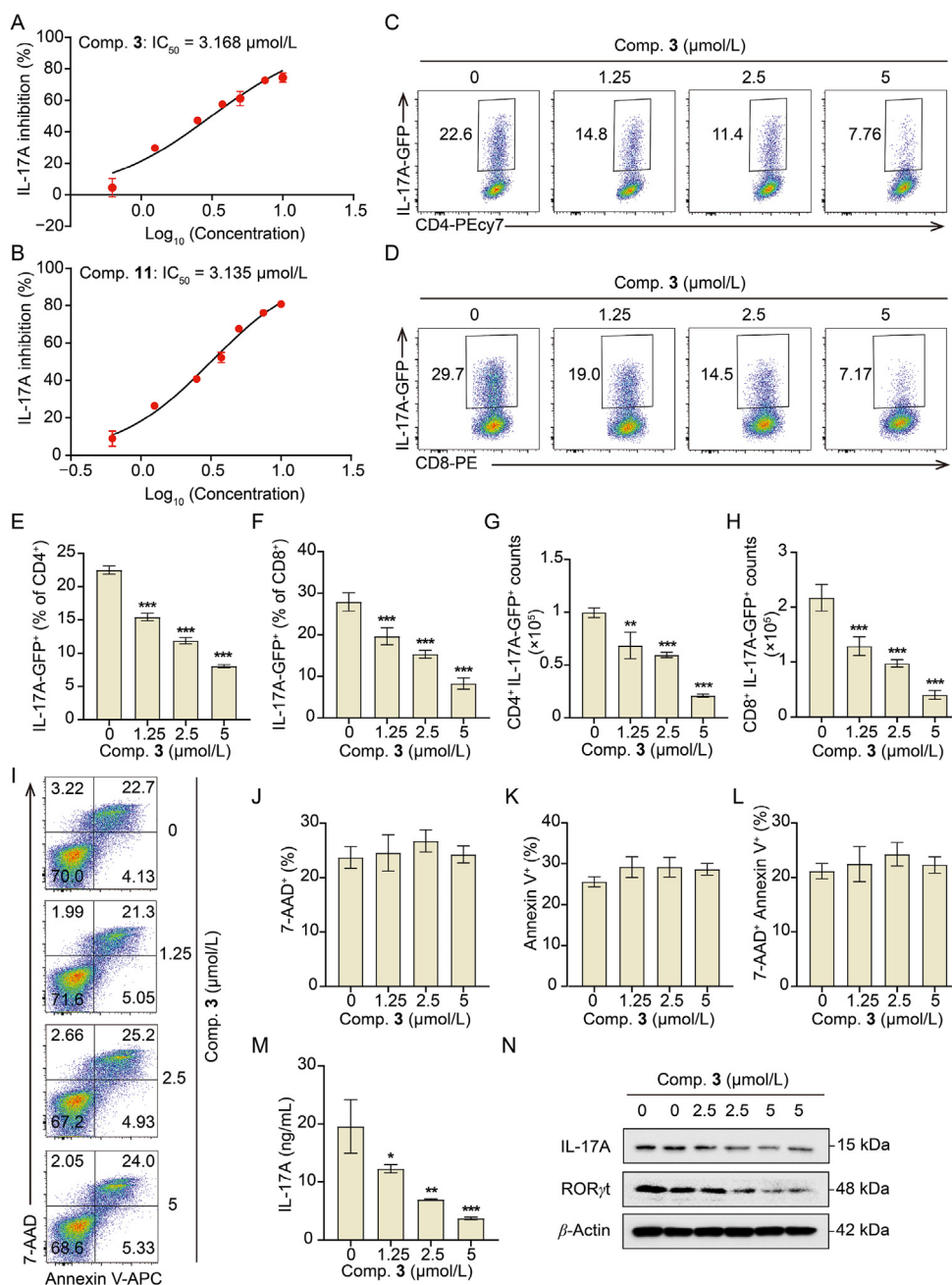


Figure 4 Effect of compound **3** on IL-17A produced from T cells under Th17-priming conditions. Splenic cells were grown in an environment conducive to Th17-priming for three days with different concentrations of compounds. (A and B) Analysis of IL-17A inhibition ratios in CD4⁺ T cells utilizing flow cytometry of compounds **3** and **11**. (C–H) Flow cytometry analysis of cell frequency and counts of IL-17A-GFP⁺ gated CD4⁺ or CD8⁺ T cells. (I–L) Quantitative analysis of cell apoptosis by 7-AAD and annexin V-APC staining. (M) ELISA was implemented to measure the levels of IL-17A in the cell culture supernatant. (N) Expression of IL-17A and RORγt assessed by Western blotting. Data were reported as mean ± SD for $n = 3$. * $P < 0.05$, ** $P < 0.01$, *** $P < 0.001$ vs. compound **3** (0 μmol/L) group.

Thus, SPs are an important class of meroterpenoids that have gained research traction. However, only eight natural aureane-type sesquiterpene tetraketides (myrothecisin C, myrothecisin D, stachyflin, acetylstachyflin, SQ-02-S-L1, SQ-02-S-L2, SQ-02-S-V1, and SQ-02-S-V2) have been reported thus far^{22,34,35}. The discovery of myrogramins A–I (**1**, **4**–**11**) has added new members to aureane-type meroterpenoids.

Mounting evidences have suggested that IL-17A, an important pro-inflammatory cytokine, performs a fundamental function

in numerous immune-related disorders and is a therapeutic target worthy of attention^{6,36}. Therefore, it is desirable to screen small molecule compounds with IL-17A inhibitory activity, for the purpose of obtain drug candidates in treating IL-17A-related diseases, like MS and PH. Based on *ex vivo* screening results, aureane-type sesquiterpene tetraketides isolated from *M. gramineum* were identified as molecules with notable IL-17A inhibitory activity and a preliminary structure–activity relationship was elucidated. Among them, compounds **1**, **3**, **4**, **10**, and **11**

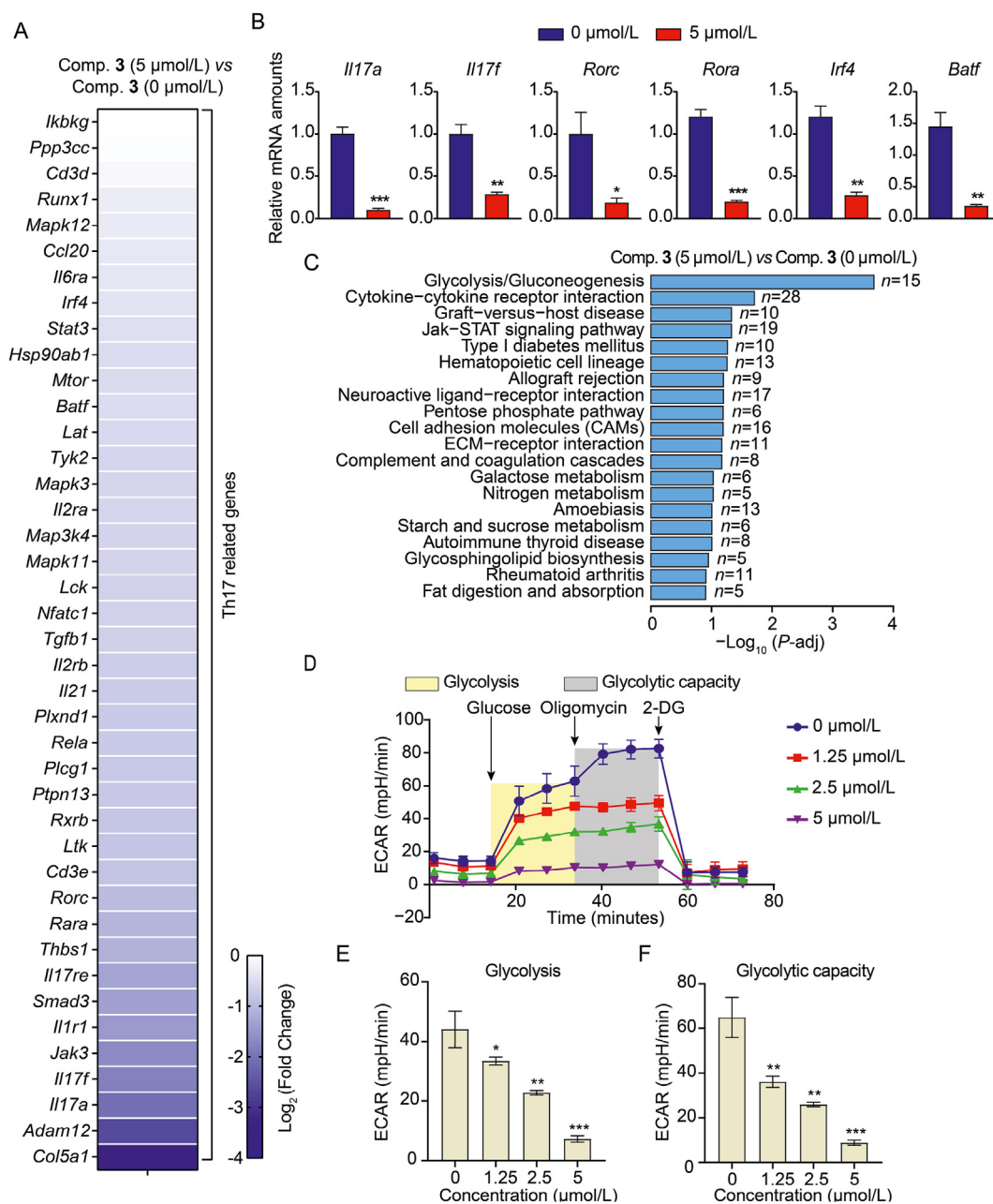


Figure 5 Compound **3** inhibits the expression of genes related to Th17 and glycolysis in the cells. (A) Heatmap shows the expression of Th17-associated genes on treatment with 5 $\mu\text{mol/L}$ compound **3** versus 0 $\mu\text{mol/L}$ compound **3**. The gene expression data were assessed by RNA-seq array. (B) qRT-PCR shows the fold change in representative Th17-related genes. (C) Top 20 signaling pathways enriched by the significant DEGs using KEGG pathway enrichment analysis. (D) ECAR was performed to compare the effect of different concentrations of compound **3** on glycolysis. (E and F) The bar graph shows glycolysis and glycolytic capacity in (D). The data were reported using the mean \pm SD for $n = 3$. * $P < 0.05$, ** $P < 0.01$, *** $P < 0.001$ vs. compound **3** (0 $\mu\text{mol/L}$) group.

significantly inhibited the generation of IL-17A in splenic cells under conditions conducive to Th17-priming. Among aureane-type sesquiterpene tetraketides with $\Delta^{1(10)}$, the activity of compound **3** was remarkably higher than those of compounds **4** and **2**, suggesting that acetylation of OH-3 and OH-8' could decrease the activity. However, among aureane-type sesquiterpene tetraketides with $\Delta^{5(10)}$, the activity of compound **11** was remarkably more than that of compound **10**, indicating that acetylation of OH-3 could increase the activity. The trend of inhibiting the production of IL-17A was $3/1 > 6/7$, indicating that a high

degree of $\text{CH}_2\text{OH}-8'$ oxidation could decrease the activity. Furthermore, the structural types of small molecule compounds that could inhibit IL-17A activity included alkaloids²¹, amides³⁷, pentacyclic triterpenes³⁸, diterpenes³⁹, steroids⁴⁰, flavonoids⁴¹, xanthenes⁴², and naphthoquinones⁴³. Among the eight natural aureane-type sesquiterpene tetraketides reported thus far, myrothecisin C and myrothecisin D show weak α -glucosidase inhibitory activity, while stachyflin, acetylstachyflin, SQ-02-S-L1, SQ-02-S-L2, SQ-02-S-V1, and SQ-02-S-V2 were reported to exert *in vitro* anti-influenza virus activity^{22,34,35}. The present

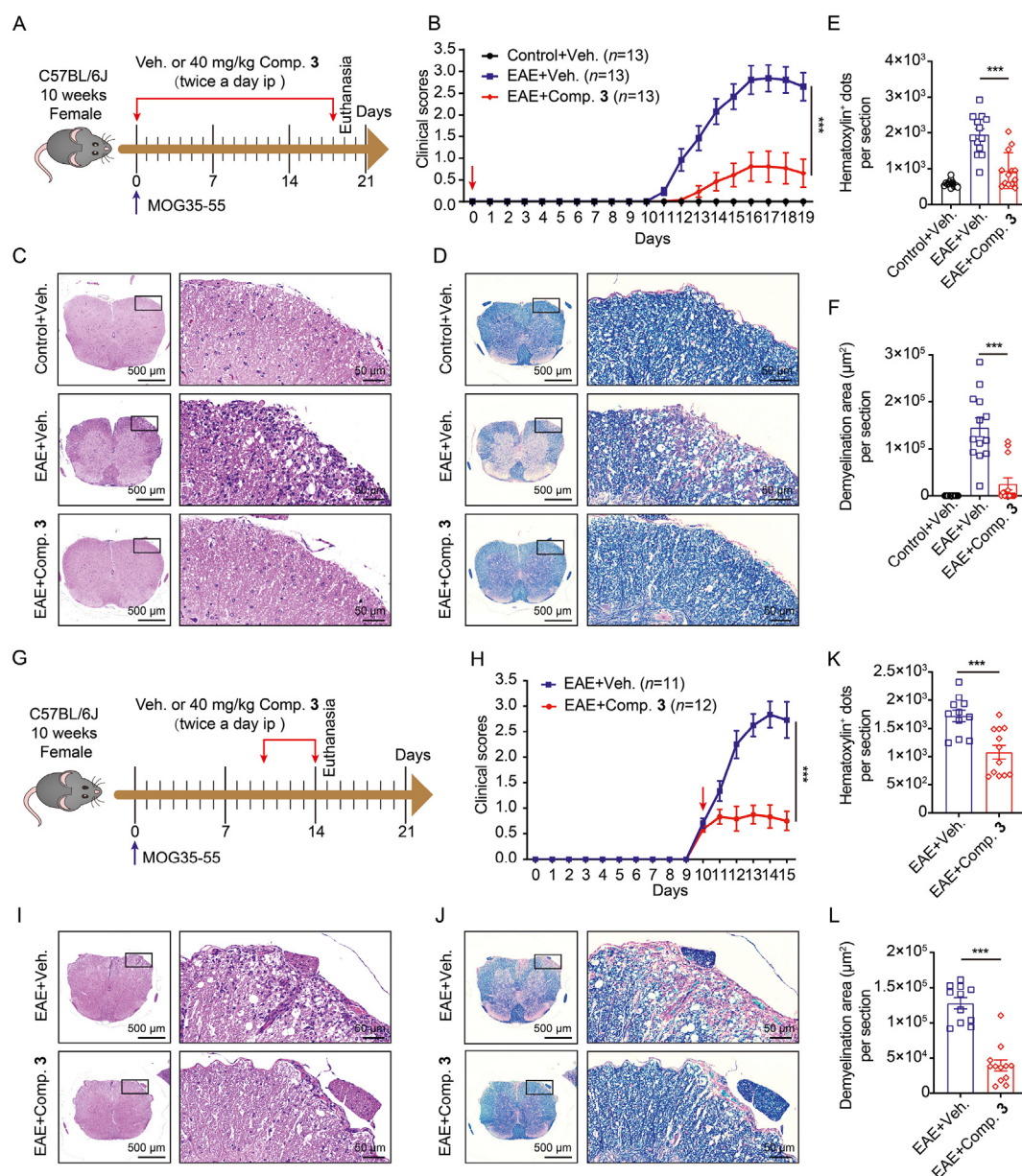


Figure 6 Compound 3 alleviates the immunopathological damages of MOG35-55-elicited EAE. (A–F) Suppression of EAE disease on treatment with compound 3 from beginning Day 0 to Day 18 post-MOG35-55 vaccination. (A) Experimental schematic of MOG35-55-elicited EAE model. (B) Clinical scores. (C and E) Illustrative hematoxylin and eosin (H&E) images of the spinal cord and statistical histograms for hematoxylin positive dots. (D and F) Illustrative luxol fast blue (LFB) staining images of the spinal cord and statistical histograms of the demyelination area. (G–L) EAE disease amelioration by compound 3 treatment from Day 10 to Day 14 post-MOG35-55 immunization. (G) Experimental schematic of EAE model. (H) Clinical scores. (I–L) Representative H&E and LFB staining images of the spinal cord and statistical histograms. Veh. represents vehicle; Comp. 3 represents compound 3. Data were represented as mean \pm SEM. *** $P < 0.001$ vs. EAE + veh. group.

study, for the first time, discovers the inhibitory activity of aureane-type sesquiterpene tetraketides on IL-17A.

In 2018, Xu et al.²² first reported the structures of myrothecisin C (2) and myrothecisin D (3) and demonstrated their weak α -glucosidase inhibitory activity (IC₅₀ values of 58 and 200 μ mol/L, respectively). Our results showed that 10 μ mol/L of compound 3 significantly inhibited IL-17A, but 2 did not show little IL-17A inhibitory activity. Although compound 3 was reported in Xu's research work, our research was the first to demonstrate that 3 had immunomodulatory properties. Considering that compound 3 had the highest fermentation productivity and showed significant IL-

17A inhibitory activity among all the aureane-type sesquiterpene tetraketides compounds 1–11, it was selected as a representative of aureane-type sesquiterpene tetraketides for subsequent studies to analyze the preliminary mechanism of its action and evaluate its efficacy on the EAE and PH animal models.

Glycolysis is the first step in breaking down of glucose molecules. It catalyzes the conversion of glucose to pyruvate through various key or rate-limiting enzymes, which plays a crucial role in ATP production and provides the basis for macromolecular biosynthesis. Multiple reports suggest glycolysis is essential during the development and differentiation of Th17 cells^{44–46}. Our

bulk RNA-sequencing results demonstrated that glycolysis/gluconeogenesis has the highest P -adj among all the pathways enriched by compound **3**. Furthermore, treatment with compound **3** significantly inhibited glycolytic activity in splenic cells cultured under Th17-priming conditions. These findings exhibited that inhibition of glycolysis could be an underlying mechanism by which compound **3** inhibited IL-17A activity. Glycolysis provides a large amount of energy and precursors for various biological

processes involved in Th17 cell differentiation, and the key enzymes of glycolysis, including hexokinase 2, pyruvate kinase muscle isozyme M2, and lactate dehydrogenase A reportedly regulate Th17 differentiation⁴⁴. Therefore, we speculate that compound **3** may affect the upstream regulators to inhibit the glycolytic processes, or directly act on the glycolytic enzymes that regulate Th17 differentiation to inhibit the production of IL-17A. Nevertheless, how glycolysis was exactly inhibited by compound

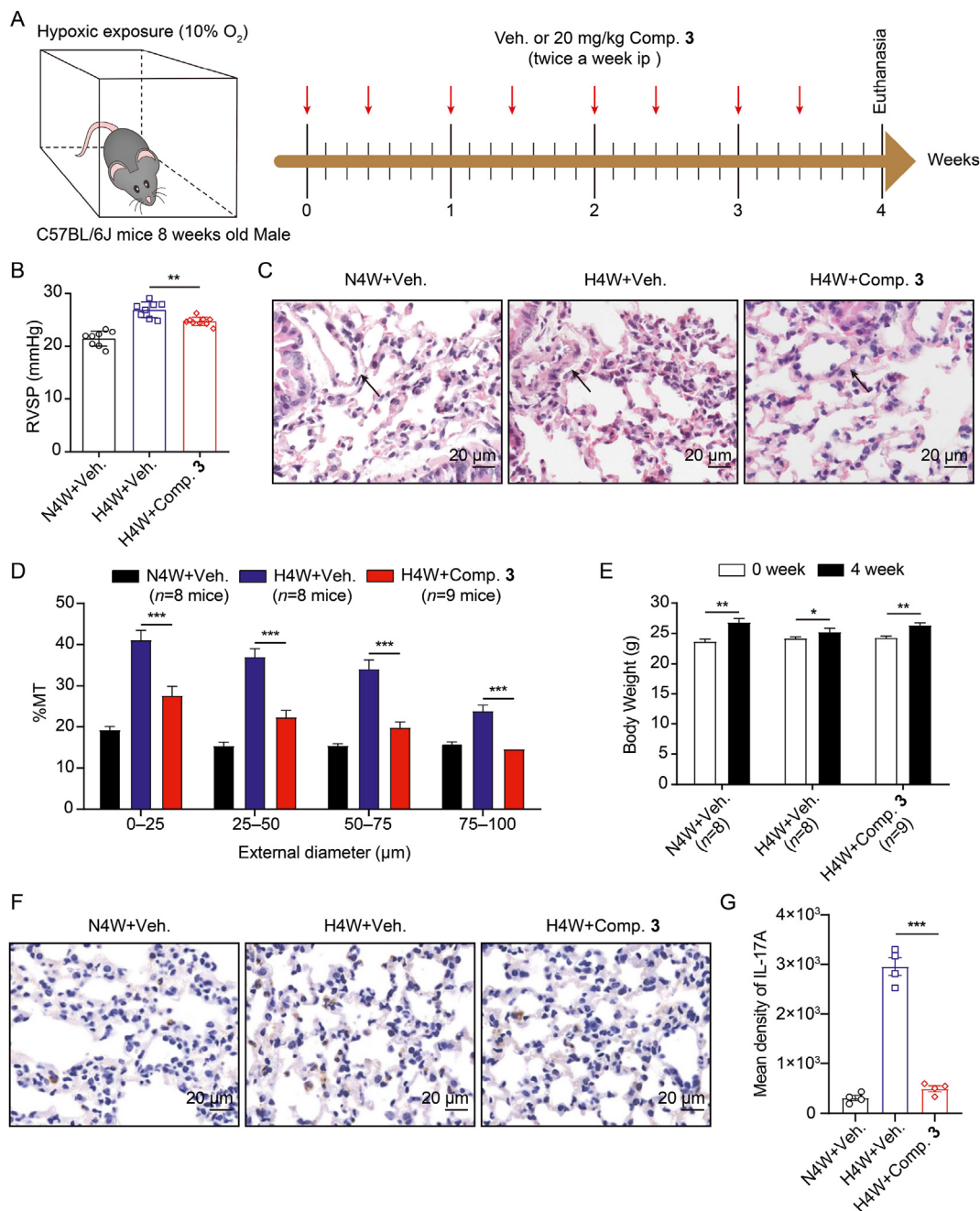


Figure 7 Compound **3** attenuates hypoxia-induced PH. (A) Experimental schematic of the hypoxia-induced PH mouse model. (B) RVSP of mice subjected to normoxia with N4W + vehicle and hypoxia with H4W + vehicle or H4W + compound **3** for four weeks. (C) A selection of representative images demonstrating the H&E staining outcomes of pulmonary arterioles. These pulmonary arterioles are denoted by arrows. (D) The percentage of the pulmonary arteriole's medial thickness relative to its exterior diameter. (E) Weight gain in the three groups. (F and G) Illustrative of IHC staining images of IL-17A in the lung tissues and statistical histograms for mean density of IL-17A expression. Veh., Comp. **3**, N4W, and H4W represent vehicle, compound **3**, normoxia for four weeks, and hypoxia for four weeks, respectively. Data were represented as mean \pm SEM. * P < 0.05, ** P < 0.01, *** P < 0.001 between indicated groups.

3 and whether the IL-17A-inhibition by compound **3** is regulated by suppression of glycolysis remain elusive, which requires a deep exploration in the future.

Further, compound **3** effectively alleviated the progression of the disease in the EAE mouse model mimicking human MS. When administered to mice beginning on the same day as MOG35-55 vaccination, compound **3**-based treatment substantially inhibited the development and immunopathology of EAE. Furthermore, the number of IL-17A⁺ cells present in the spinal cord sections of the mice decreased significantly. Interestingly, treatment of EAE mice with compound **3** after the appearance of symptoms could almost completely block its further progression. Small molecule inhibitors that target glycolysis have been reported to impair Th17 cell differentiation, thereby suppressing EAE^{45,46}. We speculate that the inhibition of glycolysis by compound **3** may be responsible for its effect on EAE-related symptoms. Our previous study has shown that IL-17A knockout mice inhibited disease progression in the hypoxia-mediated PH mouse model, whereas intravenous injection of rmIL-17A exacerbated hypoxia-induced PH¹⁵. Therefore, we reasonably speculate that targeting IL-17A could be a promising direction for treating hypoxia-induced PH. To investigate whether compound **3** can inhibit the development of hypoxia-induced PH, 20 mg/kg of compound **3** was administered to the mice twice a week under hypoxic exposure conditions (10% O₂). Hypoxia-exposed mice treated with compound **3** showed significant improvement in pulmonary artery pressure and arteriole remodeling, and the expression of IL-17A was remarkably inhibited at the lesion site of the lung compared to untreated hypoxia-exposed mice. As expected, IL-17A was an aggravating factor in hypoxia-elicited PH and participated in pulmonary vascular remodeling. Additionally, compound **3** also alleviated MCT-induced PH in rats. Therefore, compound **3** is a promising candidate for the treatment of MS and PH, as well as other IL-17A-related immune disorders. Further, whether compound **3** can mediate its action *via* multiple mechanisms rather than inhibiting IL-17A activity only to suppress PH and EAE requires further investigation.

In vitro and *in vivo* experiments demonstrated the immunomodulatory activity of aureane-type sesquiterpene tetraketides, a promising candidate with clinical applications. For further validation in a human cellular model, human naïve CD4⁺ T cells from peripheral blood mononuclear cells (PBMCs) of normal donors were extracted. DMSO or compound **3** was added to the growth medium before the cells were subjected to conditions conducive to Th17 differentiation (Supporting Information Fig. S4A). Consistent with previous results, human IL-17A levels were significantly inhibited following treatment with compound **3** (Fig. S4B and S4C). Taken together, compound **3** has promising clinical applications for treating IL-17A-related diseases.

4. Conclusions

In summary, we have isolated nine new aureane-type sesquiterpene tetraketides, myrogramins A–I (**1**, **4**–**11**), and two known ones (**2** and **3**) from *M. gramineum*, thus expanding the structural diversity of aureane-type sesquiterpene tetraketides. More importantly, our research provides a unique point of view on the immunoregulatory effects of aureane-type sesquiterpene tetraketides using *ex vivo* IL-17A inhibitory activity assay and IL-17A-related animal models of EAE and PH. Preliminary mechanistic analysis suggests that the inhibitory activity of compound **3** on IL-17A is related with the suppression of glycolysis. Ultimately, our

results suggested that aureane-type sesquiterpene tetraketides are a novel class of immunomodulators with IL-17A inhibitory activity, which have promising applications in treating IL-17A-mediated immune diseases, particularly MS and PH.

5. Experimental

5.1. Mice

IL-17A-GFP (Jax strain No. 018472) reporter mice were purchased from the Jackson Laboratory (Bar Harbor, USA). Beijing HFK Bioscience (Beijing, China) supplied the C57BL/6 J mice. The mice were kept in a specific pathogen-free environment at the Laboratory Animal Management Center at Jinan University (Guangzhou, China). Approval of all experimental protocols was granted by the Animal Experiment Committee of Jinan University. The ethical approval number for the study is No. IACUC-20191008-04.

5.2. Mouse antibodies and recombinant proteins

Anti-IFN- γ (clone XMG1.2), anti-IL-4 (clone 11B11), anti-CD28 (clone 37.51), and anti-CD3 (clone 145-2C11) were acquired from Bio X Cell (West Lebanon, NH, USA). APC annexin V apoptosis detection kit with 7-AAD was obtained from BioLegend (CA, USA). Anti-CD4 (catalog 25229 S, 1:100), anti-IL-17A (catalog 13838 S, 1:1000 for Western blotting), and anti- β -Actin (catalog 3700 S, 1:1000) were acquired from Cell Signaling Technology (MA, USA). Anti-IL-17A (catalog ab79056, 1:50 for IHC staining of the spinal cord tissues and 1:20 for IHC staining of lung tissues) and anti-ROR γ t (catalog ab207082, 1:1000) were acquired from Abcam (MA, USA). Fluorescence-conjugated anti-CD8 (clone 53-5.8), anti-GM-CSF (clone MP1-22E9), anti-IFN- γ (clone XMG1.2), anti-CD4 (clone RM4-5) were purchased from BioLegend and anti-IL-17A (clone eBio17B7) was procured from Thermo Fisher Scientific (MA, USA). rmIL-6 (catalog 216-16) was purchased from PeproTech (NJ, USA).

5.3. Splenic cells expansion culture under mouse Th17-priming conditions

Spleens were obtained from 6 to 8 weeks old IL-17A-GFP reporter mice. Splenic cells were isolated from spleens after lysis using red cell lysis buffer (Tiangen, Beijing, China). Splenic cells (1×10^6 cells/mL) were activated in 10 μ g/mL anti-CD3-coated plates with soluble 1 μ g/mL anti-CD28. Subsequently, 0.5 ng/mL recombinant human transforming growth factor- β 1.2 (rhTGF- β 1.2, catalog 304-B3, R&D Systems, MN, USA), 5 μ g/mL anti-IFN- γ , 5 μ g/mL anti-IL-4, and 40 ng/mL rmIL-6, were introduced to the culture medium for Th17-priming. Splenic cells were subjected to culturing in an Iscove's modified Dulbecco's medium (IMDM, Thermo Fisher Scientific) with 10% fetal bovine serum (Gibco, NY, USA) and 1% antibiotics at 37 °C in a 5% CO₂ atmosphere. On Day 3, the cells were collected, and subsequent analysis was performed by flow cytometry using the BD FACS-Verse instrument (BD Biosciences, CA, USA).

5.4. Flow cytometry analysis

After collecting the cells, surface marker labeling was performed by incubating them at 4 °C with particular monoclonal

antibodies for 15 min. To evaluate intracellular cytokine expression, cultured cells were stimulated in the presence of Golgi-plug (BD Biosciences) for 5 h with 1 µg/mL ionomycin (Sigma–Aldrich, MO, USA) and 50 ng/mL phorbol 12-myristate 13-acetate (Sigma–Aldrich). The intracellular staining was conducted utilizing the fixation/permeabilization kit (BD Biosciences) following the guidelines stipulated by the manufacturer. FlowJo-V10.5.3 software (BD Biosciences) was utilized to analyze the stained cells.

5.5. Extracellular acidification assays

According to the methodology outlined in our earlier research, the ECAR was calculated by employing an XF96 seahorse biosciences extracellular flux analyzer (Seahorse Biosciences, CA, USA)⁴⁷. Succinctly, DMSO- or compound **3**-treated splenic cells under Th17-priming conditions were seeded in an XF96 cell culture microplate (Seahorse Biosciences) after hydrating a sensor cartridge in XF calibrant at 37 °C throughout the night in an incubator without CO₂. The cells mentioned above were incubated in seahorse XF base medium at 37 °C for 30 min in a non-CO₂ humidified incubator with sequential inhibitor injections of 50 mmol/L 2-deoxyglucose (2-DG), 1 µmol/L oligomycin, and 10 mmol/L glucose. Finally, the glycolysis and the glycolytic capacity were detected and calculated using an XF glycolysis stress test report generator (Seahorse Biosciences).

5.6. The establishment of EAE model in mice

The EAE model was induced and evaluated as previously described⁴⁸. Briefly, 2 mg/mL of MOG35-55 (Glbiochem, Shanghai, China) was emulsified in complete Freund's adjuvant (CFA) that contained 5 mg/mL of non-viable *Mycobacterium tuberculosis* H37RA (BD Biosciences) and Freund's incomplete adjuvant (MOG35-55 was emulsified with CFA in a 1:1 volume ratio). Subsequently, 200 µg emulsified MOG35-55 was injected subcutaneously into each mouse on the posterior aspect of both ears and thigh bones on Day 0. Later, 300 ng PTX (List labs, CA, USA) in phosphate-buffered saline (PBS) was administered to each mouse *via* intravenous injection on Day 0 and Day 2. Clinical scores measuring the disease severity were scrutinized and scored daily on a scale of 0–5, as earlier illustrated⁴⁸. Compound **3** was dissolved in the vehicle (5% DMSO + 5% solutol HS 15 + 90% PBS) in 2 mg/mL, which was administered from beginning at Day 0 or Day 10 *via* ip injection at a dosage of 40 mg/kg/mouse twice daily. The control groups were administered equivalent dosages of vehicle. Solutol HS 15 was purchased from Sigma–Aldrich.

5.7. The establishment of PH model in animals

The PH animal models were induced as previously described^{15,49}. Vital River Laboratory Animal Technology Company (Beijing, China) supplied the male C57BL/6 mice that were eight weeks old and weighed 20–25 g, along with adult male Sprague–Dawley rats that weighed 250–300 g. All of the mice included in the hypoxia-induced murine PH model were kept in a light/dark cycle that lasted for 12 h, and they had unrestricted access to water and food at all times. After allowing the mice to acclimate for three days, they were placed in a chamber made of airtight plexiglass and exposed to normobaric hypoxia, which consisted of 10% oxygen, for four weeks. Mice used as controls were subjected to

identical settings, including exposure to room air. For the MCT (Sigma–Aldrich)-induced rat PH model, PH was administered by a single ip injection of 60 mg/kg MCT. Animals used as controls were administered a single ip injection of an equivalent dosage of 0.9% sodium chloride solution. Compound **3** were administered *via* ip injection at a dosage of 20 mg/kg/mouse twice a week for four weeks consecutively. The vehicle dosages that were administered to the control mice were consistent.

5.8. Histological analysis

Spinal cord and lung tissues were fixed, paraffin-embedded, and sectioned as previously described^{15,48}, followed by histological staining. SlideViewer 2.5 (<https://www.3dhistech.com>) was used for the reading and preliminary image processing of spinal cord and lung tissue sections. Next, image-Pro Plus 6.0 was utilized in quantifying the hematoxylin positive dots for each H&E section, the demyelination area per LFB section, the number of infiltrating CD4⁺ T cells per IHC section, and the mean density of IL-17A. The white matter of the spinal cord was selected to statistically analyze the pathological alteration.

5.9. Statistical analysis

GraphPad Prism version 9 was employed to undertake all analyses involving statistical data. Two-tailed unpaired student's *t*-tests were utilized for comparison involving the two groups. To examine the differences involving groups exceeding two, a one-way analysis of variance (ANOVA) was conducted. Two-way ANOVA was implemented for the analysis of data containing two independent parameters. Data from cellular level and animal level experiments were presented as mean ± SD and mean ± SEM, respectively. **P* < 0.05, ***P* < 0.01, and ****P* < 0.001 denote statistically significant variation.

Acknowledgments

This work is supported by the National Key Research and Development Program of China (2018YFA0903200, 2018YFA0903201, and 2020YFA0803502), the National Natural Science Foundation of China (81925037, U22A20371, 31830021, 32030036, and 82270055) and the 111 Project (B16021, China). National High-level Personnel of Special Support Program (2017RA2259, China), Guangdong International Science and Technology Cooperation Base (2021A0505020015, China), Innovative and Research Teams Project of Guangdong Higher Education Institution (2021KCXTD001, China), Local Innovative and Research Teams Project of Guangdong Pearl River Talents Program (2017BT01Y036, China), and Guangdong Natural Science Funds for Distinguished Young Scholar (2021B1515020065, China). We would like to thank Guangchao Cao and Yue Zhao of Jinan University (China) for helping with EAE modeling and guiding us with the histological analysis, respectively. We are also grateful to the Guangzhou Blood Centre (China) for providing human peripheral blood samples from healthy donors.

Author contributions

Zhinan Yin, Hao Gao, and Chen Wang conceived this research and revised the manuscript. Xin Tang, Chuanxi Wang, Lei Wang, Runqiao Kuang, and Zhenhua Li analyzed the data and wrote the

manuscript. Xin Tang, Feifei Ren, Zhenhua Li, Hengwen Yang, Yiming Chen, and Xiuqing Wu performed the *in vitro* and *in vivo* bioactivity assays except for the PH model. Chuanxi Wang, Runqiao Kuang, Guodong Chen, and Xue Han performed the separation, structural identification, and enrichment of the compounds. Lei Wang and Jie Liu conducted the PH efficacy evaluation.

Conflict of interest

The authors state that there are no conflicts of interest involved.

Appendix A. Supporting information

Supporting data to this article can be found online at <https://doi.org/10.1016/j.apsb.2023.03.017>.

References

- McGeachy MJ, Cua DJ, Gaffen SL. The IL-17 family of cytokines in health and disease. *Immunity* 2019;**50**:892–906.
- Harrington LE, et al. Interleukin 17-producing CD4⁺ effector T cells develop via a lineage distinct from the T helper type 1 and 2 lineages. *Nat Immunol* 2005;**6**:1123–32.
- Miossec P, Kolls JK. Targeting IL-17 and Th17 cells in chronic inflammation. *Nat Rev Drug Discov* 2012;**11**:763–76.
- Ivanov, et al. The orphan nuclear receptor ROR γ t directs the differentiation program of proinflammatory IL-17⁺ T helper cells. *Cell* 2006;**126**:1121–33.
- Singh RP, et al. Th17 cells in inflammation and autoimmunity. *Autoimmun Rev* 2014;**13**:1174–81.
- Zwicky P, Unger S, Becher B. Targeting interleukin-17 in chronic inflammatory disease: a clinical perspective. *J Exp Med* 2020;**217**.
- Moser T, Akgun K, Proschmann U, Sellner J, Ziemssen T. The role of TH17 cells in multiple sclerosis: therapeutic implications. *Autoimmun Rev* 2020;**19**:102647.
- Maston LD, et al. Central role of T helper 17 cells in chronic hypoxia-induced pulmonary hypertension. *Am J Physiol Lung Cell Mol Physiol* 2017;**312**:L609–24.
- McGinley MP, Goldschmidt CH, Rae-Grant AD. Diagnosis and treatment of multiple sclerosis: a review. *JAMA* 2021;**325**:765–79.
- Stromnes IM, Goverman JM. Active induction of experimental allergic encephalomyelitis. *Nat Protoc* 2006;**1**:1810–9.
- McGinley AM, Edwards SC, Raverdeau M, Mills KHG. Th17 cells, $\gamma\delta$ T cells and their interplay in EAE and multiple sclerosis. *J Autoimmun* 2018;**87**:97–108.
- Poch D, Mandel J. Pulmonary hypertension. *Ann Intern Med* 2021;**174**:ITC49–64.
- Hautefort A, et al. T-helper 17 cell polarization in pulmonary arterial hypertension. *Chest* 2015;**147**:1610–20.
- Gaowa S, et al. Effect of Th17 and Treg axis disorder on outcomes of pulmonary arterial hypertension in connective tissue diseases. *Mediat Inflamm* 2014;**2014**:247372.
- Wang L, et al. Targeting IL-17 attenuates hypoxia-induced pulmonary hypertension through downregulation of β -catenin. *Thorax* 2019;**74**:564–78.
- Genovese MC, et al. Safety of ixekizumab in adult patients with plaque psoriasis, psoriatic arthritis and axial spondyloarthritis: data from 21 clinical trials. *Rheumatology* 2020;**59**:3834–44.
- Kolbinger F, et al. Secukinumab for the treatment of psoriasis, psoriatic arthritis, and axial spondyloarthritis: physical and pharmacological properties underlie the observed clinical efficacy and safety. *Pharmacol Ther* 2022;**229**:107925.
- Zhang BD, Domling A. Small molecule modulators of IL-17A/IL-17RA: a patent review (2013–2021). *Expert Opin Ther Pat* 2022;**32**:1–13.
- Li ZH, Liu T, He XX, Bai C. The evolution paths of some representative scaffolds of ROR γ t modulators, a perspective from medicinal chemistry. *Eur J Med Chem* 2022;**228**:113962.
- Gege C. Retinoic acid-related orphan receptor gamma t (ROR γ t) inverse agonists/antagonists for the treatment of inflammatory diseases—where are we presently?. *Expet Opin Drug Discov* 2021;**16**:1517–35.
- Glenn JD, Pantoja IM, Caturegli P, Whartenby KA. MYMD-1, a novel alkaloid compound, ameliorates the course of experimental autoimmune encephalomyelitis. *J Neuroimmunol* 2020;**339**:577115.
- Xu YC, et al. Meroterpenoids and isocoumarinoids from a *myrothecium* fungus associated with *Apocynum venetum*. *Mar Drugs* 2018;**16**:363.
- Zhu YY, et al. New opportunities and challenges of natural products research: when target identification meets single-cell multiomics. *Acta Pharm Sin B* 2022;**12**:4011–39.
- Milovanovic J, et al. Interleukin-17 in chronic inflammatory neurological diseases. *Front Immunol* 2020;**11**:947.
- Speck K, Magauer T. The chemistry of isoindole natural products. *Beilstein J Org Chem* 2013;**9**:2048–78.
- Marcos IS, Conde A, Moro RF, Basabe P, Diez D, Urones JG. Quinone/hydroquinone sesquiterpenes. *Mini-Reviews Org Chem* 2010;**7**:230–54.
- Geris R, Simpson TJ. Meroterpenoids produced by fungi. *Nat Prod Rep* 2009;**26**:1063–94.
- Jiao WH, et al. Bioactive sesquiterpene quinols and quinones from the marine sponge *Dysidea avara*. *RSC Adv* 2015;**5**:87730–8.
- Li Y, Wu CM, Liu D, Proksch P, Guo P, Lin W. Chartaractams A–P, phenylspirodrimanes from the sponge-associated fungus *Stachybotrys chartarum* with antihyperlipidemic activities. *J Nat Prod* 2014;**77**:138–47.
- Hagiwara K, et al. Puupehenol, a potent antioxidant antimicrobial meroterpenoid from a Hawaiian deep-water *Dactylosporgia* sp. sponge. *J Nat Prod* 2015;**78**:325–9.
- Novakovic I, Anđelkovic U, Zlatovic M, Gasic MJ, Sladic D. Bioconjugate of lysozyme and the antibacterial marine sesquiterpene quinone avarone and its derivatives. *Bioconjugate Chem* 2012;**23**:57–65.
- Ma XH, et al. Phenylspirodrimanes with anti-HIV activity from the sponge-derived fungus *Stachybotrys chartarum* MXH-X73. *J Nat Prod* 2013;**76**:2298–306.
- Daletos G, et al. Cytotoxic and protein kinase inhibiting nakijiquinones and nakijiquinols from the sponge *Dactylosporgia meta-chromia*. *J Nat Prod* 2014;**77**:218–26.
- Minagawa K, Kouzuki S, Yoshimoto J, Kawamura Y, Tani H, Iwata T, et al. Stachyflin and acetylstachyflin, novel anti-influenza A virus substances, produced by *Stachybotrys* sp. RF-7260. *J Antibiot (Tokyo)* 2002;**55**:155–64.
- Minagawa K, et al. Novel stachyflin derivatives from *Stachybotrys* sp. RF-7260. *J Antibiot (Tokyo)* 2002;**55**:239–48.
- Stockinger B. Lumpers and splitters: birth of Th17 cells. *J Exp Med* 2021;**218**:e20210645.
- Sabnis RW. Novel difluorocyclohexyl derivatives as IL-17 modulators for treating inflammatory and autoimmune diseases. *ACS Med Chem Lett* 2022;**13**:160–1.
- Chen LJ, et al. SZB120 exhibits immunomodulatory effects by targeting eIF2 α to suppress Th17 cell differentiation. *J Immunol* 2021;**206**:953–62.
- Zhang C, Ma K, Yang YM, Wang FQ, Li WY. Glaucoalyxin A suppresses inflammatory responses and induces apoptosis in TNF- α -induced human rheumatoid arthritis via modulation of the STAT3 pathway. *Chem Biol Interact* 2022;**352**:109684.
- Ladurner A, Schwarz PF, Dirsch VM. Natural products as modulators of retinoic acid receptor-related orphan receptors (RORs). *Nat Prod Rep* 2021;**38**:757–81.

41. Wei CB, Tao K, Jiang R, Zhou LD, Zhang QH, Yuan CS. Quercetin protects mouse liver against triptolide-induced hepatic injury by restoring Th17/Treg balance through Tim-3 and TLR4-MyD88-NF-kappaB pathway. *Int Immunopharm* 2017;**53**:73–82.
42. Zhou XQ, et al. α -Mangostin attenuates pristane-induced lupus nephritis by regulating Th17 differentiation. *Int J Rheum Dis* 2020;**23**:74–83.
43. Kono M, et al. Pyruvate kinase M2 is requisite for Th1 and Th17 differentiation. *JCI Insight* 2019;**4**:e127395.
44. Shen HX, Shi LZ. Metabolic regulation of Th17 cells. *Mol Immunol* 2019;**109**:81–7.
45. Bechara R, McGeachy MJ, Gaffen SL. The metabolism-modulating activity of IL-17 signaling in health and disease. *J Exp Med* 2021;**218**.
46. Kornberg MD, et al. Dimethyl fumarate targets GAPDH and aerobic glycolysis to modulate immunity. *Science* 2018;**360**:449–53.
47. Li ZH, Tang X, Zhu LF, Qi XJ, Cao G, Lu G. Cytotoxic screening and transcriptomics reveal insights into the molecular mechanisms of trihexyl phosphate-triggered hepatotoxicity. *Environ Sci Technol* 2020;**54**:11464–75.
48. Cao GC, et al. Long-term consumption of caffeine-free high sucrose cola beverages aggravates the pathogenesis of EAE in mice. *Cell Discov* 2017;**3**:17020.
49. Yang YC, et al. Discovery of highly selective and orally available benzimidazole-based phosphodiesterase 10 inhibitors with improved solubility and pharmacokinetic properties for treatment of pulmonary arterial hypertension. *Acta Pharm Sin B* 2020;**10**:2339–47.